16 A time-dependent quantal approach to electronic transitions in atomic collisions

T. Kirchner[1], H. J. Lüdde[2] and M. Horbatsch[3]
[1]Institut für Theoretische Physik, TU Clausthal, Leibnizstraße 10, D-38678
Clausthal-Zellerfeld, Germany; [2]Institut für Theoretische Physik, Johann Wolfgang
Goethe-Universität, Robert-Mayer-Straße 8, D-60054 Frankfurt, Germany
[3]Department of Physics and Astronomy, York University, Toronto, Ontario
M3J 1P3 Canada

Abstract

This article reviews recent advances in the theoretical description of ion-atom collisions, which were made on the basis of a quantum mechanical description of the electron dynamics and a classical treatment of the heavy particle motion. It is explained how time-dependent density functional theory provides a suitable framework for the discussion of single- and many-electron effects and processes and how the recently developed basis generator method accomplishes the task of atomic orbital propagation including the electron continuum. Results for ionisation and electron transfer are discussed for a variety of collision systems, covering positively and negatively charged projectiles, and targets ranging from hydrogen to argon atoms. Emphasis is put on the

Correspondence/Reprint request: Prof. Dr. Tom Kirchner, Institut für Theoretische Physik, TU Clausthal, Leibnizstraße 10
D-38678 Clausthal-Zellerfeld, Germany. E-mail: tom.kirchner@tu-clausthal.de

analysis of different facets of the electron interaction and dynamics, which are revealed by comparing different models among themselves and with experimental data.

1. Introduction

Atomic collisions and the behaviour of the participating electrons in particular, have been investigated experimentally and theoretically for many years. Such studies fostered a wealth of applications spanning such widely differing areas as plasma diagnostics [1], atmospheric science [2], radiobiolgy and tumor therapy [3]. Moreover, the subject has contributed considerably to our general understanding of interacting few-body systems which are governed by the laws of quantum mechanics.

On the experimental side a major breakthrough in recent years has been the development of the so-called *cold target recoil ion momentum spectroscopy* (COLTRIMS) [4]. This technique aims at the determination of the momenta of all free particles in the exit channel of a collision in order to obtain a complete picture of the collision dynamics. Several groups around the world are currently using variants and extensions of COLTRIMS to investigate, e.g., single and multiple electron emission from atoms and molecules induced by photons, electrons, and ions, charge-transfer in ion-atom collisions, and more recently, ionisation of atoms and molecules by intense short laser pulses. The most recent results are reviewed in [5].

The theoretical description of these modern atomic collision experiments turned out to be very demanding. Only recently has it become possible to calculate successfully for one- and two-electron scattering systems the fine details of electron removal processes (see, e.g., [6, 7] and the recent review [8]). A similar situation is encountered in the determination of accurate total cross sections at intermediate impact energies, where, in general, different reaction channels are coupled [9, 10]. A large body of experimental data is still unexplained, particularly if systems with *several* active electrons are considered. This reflects the complexity and the intricacies of the quantum many-body problem in situations, in which energy and momentum are available to induce inelastic transitions. A simple estimate shows that despite the tremendous increase of available computer power the full solution of the Schrödinger equation that describes a many-electron scattering problem will be out of reach for some time to come [11]. The main problem is, of course, the two-body nature of the electron-electron interaction, which couples the coordinates of all electrons and prohibits the factorisation of the many-electron wave function into several one-electron states. Thus, it is the presence of electron correlation effects which makes the theoretical treatment of such collision systems so challenging.

The present article deals with ion-atom collisions at intermediate impact energies, where electron excitation, transfer, and ionisation processes compete with each other and call for a nonperturbative theoretical treatment. Several approaches have been proposed in recent years with the aim to reduce the computational complexity of a complete many-body treatment without neglecting electronic correlations entirely [11, 12, 13]. Up to now, however, only two-electron scattering systems have been addressed in these frameworks, which indicates their still demanding nature.

In order to deal also with *true* many-electron systems we have approached the problem from a different perspective, based on the concepts of time-dependent density functional theory (TDDFT). The calculations are performed with the newly developed

basis generator method (BGM), and special attention is given to the question of how to extract the physical information from the propagated equations. Thus, we have a new methodology to describe systems involving one, two, and many active electrons. The present paper reviews this approach with emphasis on the discussion of results, which are selected from a series of recent papers.

The salient points of the theoretical description are summarized in Sec. 2. In Sec. 3 we present results for collision systems with one active electron to illustrate the capabilities of the BGM. Section 4 is devoted to many-electron systems. First, we discuss one-electron processes in Sec. 4.1, and then we consider multiple-electron processes in Secs. 4.2 and 4.3. The results are summarised in Sec. 5. Some extensions of the approach, such as the discussion of *laser-assisted* collisions are briefly sketched in Sec. 6 together with a short outlook on future investigations. Atomic units ($\hbar = m_e = e = 1$) are used throughout the article unless indicated otherwise.

2. Theory

Within the well-established semiclassical approximation (SCA) [14] ion-atom collisions are viewed as time-dependent processes, in which the quantum dynamics of the electrons are governed by their internal interactions and by the Coulomb fields of the classically moving nuclei. For collision energies above $E_P \approx 1$ keV/amu the projectile motion is commonly approximated by a straight-line trajectory $\vec{R}(t) = (b, 0, \upsilon_p t)$ with impact parameter b and constant velocity υ_P. In this framework one has to solve a time-dependent Schrödinger equation (TDSE) for the many-electron state $\Psi(t)$

$$\mathrm{i}\,\partial_t \Psi(t) = \hat{H}(t)\Psi(t) \,, \tag{1}$$

with a Hamiltonian

$$\hat{H}(t) = \hat{T} + \hat{W} + \hat{V}(t) \tag{2}$$

that includes the kinetic energy

$$\hat{T} = \sum_{j=1}^{N} \left(-\frac{1}{2}\nabla_j^2\right) \,, \tag{3}$$

the electron-electron interaction

$$\hat{W} = \sum_{i<j=1}^{N} \frac{1}{|\vec{r_i} - \vec{r_j}|} \,, \tag{4}$$

and the Coulomb potentials of the target and the projectile nuclei with charges Z_T and Z_P, respectively

$$\hat{V}(t) = \sum_{j=1}^{N} \left(\frac{-Z_T}{r_j} + \frac{-Z_P}{|\vec{r}_j - \vec{R}(t)|} \right) \; . \tag{5}$$

Spin-dependent interactions and relativistic effects are neglected, but we note that the electron spin enters the treatment via the spin-statistics theorem as the requirement that the many-electron wave function $\Psi(t)$ be antisymmetric (see Sec. 2.3).

The task is now to propagate $\Psi(t)$ from a given initial state

$$\Psi(t_0) = \Psi_0 \tag{6}$$

to a final time $t = t_f$, which is large enough to ensure convergence with respect to time for the observables of interest. At t_f we wish to calculate impact-parameter-dependent probabilities for transitions to final states Φ_f

$$P_f(b) = |\langle \Phi_f | \Psi \rangle|^2_{t=t_f} \tag{7}$$

and corresponding total cross sections

$$\sigma_f = 2\pi \int_0^\infty b P_f(b) \mathrm{d}b \; . \tag{8}$$

Cross sections which are differential in the projectile deflection can also be calculated within the SCA by a Bessel transform of the transition *amplitudes* [15]. In this article, however, we will be mainly concerned with total cross sections.

In the next two subsections we explain briefly how the time-dependent many-electron problem (1) is mapped onto a set of single-particle equations by virtue of the Runge-Gross theorem of TDDFT and how we solve these equations. After that, we describe in Sec. 2.3 how probabilities for many-electron transitions (7) can be extracted from the single-particle solutions.

2.1 Time-dependent density functional theory

A nonrelativistic electronic system coupled to a time-dependent classical environment with which it exchanges energy is described by the TDSE (1). The Hamiltonian can generally be decomposed according to Eq. (2) into a universal time-independent part including the kinetic energy (3) and the mutual Coulomb repulsion between the electrons (4), and the system-specific external potential [cf. Eq. (5)]

$$\hat{V}(t) = \sum_{j=1}^{N} v(\vec{r}_j, t) \; . \tag{9}$$

The latter characterises the particular geometry as well as the explicit time dependence of the electronic system due to its interaction with the classical environment (in our case the classically moving nuclei).

The basic idea behind density functional theory (DFT) is the existence of a unique map between the many-electron state $\Psi(t)$ and the one-particle density n of the system

$$n(\vec{r}, t) = N \sum_s \int \mathrm{d}^4 x_2 \ldots \mathrm{d}^4 x_N \, |\Psi(\vec{x}_1, \ldots \vec{x}_N, t)|^2 \,, \tag{10}$$

where $\vec{x}_j = (\vec{r}, s)$ denotes coordinates and spin of the j-th electron and $\mathrm{d}^4 x_j$ indicates summation over spin and integration over space coordinates, respectively (for reviews on time-dependent DFT see [16, 17, 18, 19]. A comprehensive introduction to stationary DFT can be found in [20].).

The Runge–Gross theorem [21] proves the uniqueness of the functional $\Psi[n](t)$ up to a merely time-dependent phase factor, if the many-electron system evolves from a non-degenerate initial ground state. This is a very powerful statement. It implies that, in principle, the complete information that is contained in the many-electron wave function can be reconstructed from the one-particle density (10), i.e., it suffices to calculate the latter in order to evaluate the observables of the many-electron system.

The gist of DFT is, thus, the determination of the exact one-particle density without calculating the many-electron wave function. In the Kohn-Sham (KS) scheme, which represents the most popular DFT scheme one assumes that the density can be represented in terms of a set of N orbitals $\{\varphi_j, j = 1, \ldots N\}$

$$n(\vec{r}, t) = \sum_{j=1}^{N} |\varphi_j(\vec{r}, t)|^2 \,, \tag{11}$$

which fulfil single-particle Schrödinger — so-called time-dependent Kohn-Sham (TDKS) — equations of the form

$$\mathrm{i}\, \partial_t \varphi_j(\vec{r}, t) = \hat{h}(t) \varphi_j(\vec{r}, t) = \left(\frac{-\nabla^2}{2} + v_{\mathrm{KS}}(\vec{r}, t) \right) \varphi_j(\vec{r}, t) \,, j = 1, \ldots N \,. \tag{12}$$

Thus, the many-electron problem is mapped to a set of single-particle equations. The KS orbitals $\{\varphi_j, j = 1, \ldots N\}$ have no physical meaning; it is the density n which fully determines the time evolution of the N-particle system.

The Kohn-Sham potential v_{KS} is a unique functional of n which is again a consequence of the Runge–Gross theorem. However, this functional is not known exactly. One usually separates the KS potential into an electrostatic part, which consists of the external (Coulomb) interaction $v(\vec{r}, t)$ and the Hartree potential v_{H} that accounts for the screening of the external potential due to the electrons, and an intrinsic quantum part v_{xc}, the *exchange-correlation* potential

$$
\begin{aligned}
v_{\mathrm{KS}}[n](\vec{r}, t) &= v(\vec{r}, t) + v_{\mathrm{H}}[n](\vec{r}, t) + v_{\mathrm{xc}}[n](\vec{r}, t) \\
v_{\mathrm{H}}[n](\vec{r}, t) &= \int \mathrm{d}^3 r' \frac{n(\vec{r}', t)}{|\vec{r} - \vec{r}'|} \,.
\end{aligned}
\tag{13}
$$

For time-dependent systems the inclusion of correlation is still out of reach restricting applications to the level of an exchange-only (x-only) approximation v_{x} of the KS

potential. The *optimised* (*effective*) *potential method* (OEP → OPM) originally introduced by Talman and Shadwick [22] and frequently applied to static problems [23] provides a scheme to exactly determine the exchange potential as a unique functional of *n*. The fact that this functional is local in space clearly demonstrates the merit of DFT in comparison with the Hartree-Fock (HF) method.

2.2 The basis generator method (BGM)

The numerical solution of the time-dependent Schrödinger or KS equations (12) for an electronic system is quite involved. The long-range behaviour of the Coulomb interaction requires numerical methods of sufficient accuracy and stability over large time scales to account for the considerable delocalisation of the electronic density during the collision process. As a consequence, a broad spectrum of numerical methods has been developed in particular for ion-atom collisions: (i) lattice techniques discretising the TDSE in configuration space [24], momentum space [25] or a combination thereof based on Fast-Fourier Transform algorithms [6, 26], (ii) expansion methods relying on single-centre [27, 28, 29, 30] or two-centre [31] basis sets, (iii) the hidden crossing method [32] valid for adiabatic collisions, and with a broad range of applications (iv) the classical trajectory Monte Carlo method [33, 34, 35], which simulates the electronic system in terms of a statistical ensemble of classical point charges.

While lattice techniques and expansion methods are motivated by making an attempt at the completeness of the representation of the Hilbert space $\mathcal{H}$, the philosophy of the *basis generator method* (BGM) [36] is different. Given that the time-dependent state $|\Psi(t)\rangle$ defines a one-dimensional subspace of $\mathcal{H}$ completeness is not an essential quality criterion: if one could generate a dynamic subspace embedding the path of the exact state like a 'hose', one could dramatically reduce the effort needed for the numerical solution of the TDSE.

The BGM starts with a finite set of eigenfunctions of the undisturbed system

$$\begin{aligned}
\hat{h}_0|\phi_v^0\rangle &= \varepsilon_v|\phi_v^0\rangle\,, \quad v = 1,\ldots,V \\
\hat{h}_0 &= \frac{-\nabla^2}{2} + v_{\text{KS}}(\vec{r},t_0)\,,
\end{aligned} \tag{14}$$

which is called the *generating basis*. Successive mapping of these functions with the single-particle Schrödinger operator $\hat{O} = \hat{h}(t) - i\partial_t$ generates a hierarchy of V–dimensional subspaces of the Hilbert space

$$\begin{aligned}
|\phi_v^u(t)\rangle &= \hat{O}|\phi_v^{u-1}(t)\rangle \\
&= \hat{O}^u|\phi_v^0\rangle\,, \quad v = 1,\ldots,V\,, \quad u = 1,\ldots,U\,,
\end{aligned} \tag{15}$$

with the following properties:

- The set of states $\{|\phi_v^u(t)\rangle, v = 1,\ldots,V; u = 0,\ldots,U\}$ is linearly independent and forms a dynamic subspace $\mathcal{A}^{UV}$ of $\mathcal{H}$.

- For $u < U$ the states of Eq. (15) interact merely *within* the hierarchy of finite subspaces. This means that only the states belonging to the U-th subset couple to the infinite complementary space of $\mathcal{A}^{UV}$. If these states are not accessed during the time propagation, the pseudostates (15) enable an *exact* representation of the TDSE.

The structure of the states defined in Eq. (15) becomes rather involved with increasing order u. For a given interaction $\hat{v}(t)$ it is, thus, useful to introduce an alternative set of states $\{|\chi_\nu^\mu(t)\rangle, \nu = 1, \ldots, N, \mu = 0, \ldots, M\}$ with

$$|\chi_\nu^\mu(t)\rangle = \hat{v}(t)^\mu |\chi_\nu^0\rangle , \tag{16}$$

generating a second finite model space $\mathcal{R}^{MN}$. It can be shown [37] that for any given (U, V) there exist finite numbers $M(U, V)$ and $N(U, V)$ such that $\mathcal{A}^{UV} \subseteq \mathcal{R}^{MN}$ if the following conditions are fulfilled:

- The generating basis of Eq. (14) (including the physical initial condition) is contained in $\mathcal{R}^{0N}$;

- The operator $\hat{O}$ maps each state $|\chi_\nu^\mu(t)\rangle$ onto a *finite* linear combination $\mathcal{L}_{\mu\nu}$ of the states $\{|\chi_\lambda^\kappa(t)\rangle\}$

$$\hat{O}|\chi_\nu^\mu(t)\rangle = \mathcal{L}_{\mu\nu}(\{|\chi_\lambda^\kappa(t)\rangle\}) \in \left[|\chi_\lambda^\kappa(t)\rangle, \ \lambda = 1, \ldots, L, \ \kappa = 0, \ldots, K\right], \tag{17}$$

where $L = L(\mu, \nu)$ and $K = K(\mu, \nu)$.

For potentials $\hat{v}(t)$ that can be expanded in a power series of a pure Coulomb potential — which has to be regularised at $\vec{r} \to 0$ (see Sec. 3) — the space $\mathcal{R}^{MN}$ includes the optimised space $\mathcal{A}^{UV}$. The KS orbitals $\{\varphi_j, j = 1, \ldots N\}$ are then represented in terms of the states (16) and the resulting set of ordinary differential equations is eventually solved by standard methods.

2.3 Extraction of many-electron transition probabilities

The existence of a unique map between the many-electron state $\Psi(t)$ and the one-particle density n implies that, in principle, any many-electron observable can be derived directly from n. In practice, however, the usefulness of this statement is limited, since only a few functionals for accessible observables are known exactly. Important examples are the so-called *net probabilities*, which correspond to the average numbers of electrons which are, e.g., bound to the target, to the projectile, or released to the continuum. They are given asymptotically as integrals of n over the corresponding regions in coordinate space [19].

Less global quantities, however, can at present only be computed in the no-correlation limit of TDDFT, in which the KS orbitals are assumed to carry the physical information about the active electrons. This corresponds to an analysis of the collision

system at the level of the independent particle model (IPM)[1]. Within the IPM, one starts with the calculation of single-particle probability amplitudes for elastic scattering, excitation, and capture by projecting the KS orbitals at $t = t_f$ onto a set of bound target and projectile states. With the assumption that the propagated and the final many-electron states are single Slater determinants one finds that the inclusive probability $P_{f_1, \ldots, f_q}$ of finding q out of N electrons in states labeled $f_1, \ldots, f_q$, while the other N–q electrons are not detected can be expressed as a $q \times q$ determinant of the one-particle density matrix [39]

$$P_{f_1, \ldots, f_q} = \det(\langle f_1|\hat{n}|f_1 \rangle \cdots \langle f_q|\hat{n}|f_q \rangle) \,. \tag{18}$$

Higher inclusive probabilities, such as q-particle ionisation P_q^{ion}, capture P_q^{cap}, and loss $P_q^{\mathrm{loss}} = P_q^{\mathrm{ion}} + P_q^{\mathrm{cap}}$ can be expressed as ordered sums of the probabilities (18) [40].

In many situations, namely when the number of final states which correspond to the observable of interest is large, the determinantal structure of the transition probabilities can be neglected. In these cases one arrives at multinomial expressions of single-particle transition probabilities, which have been used widely over many years [41, 42]. If p_i denotes the single-particle probability, e.g., for ionisation of an electron from the i-th shell the probability for q-fold ionisation is given as

$$P_q^{\mathrm{ion}} = \sum_{q_1, \ldots, q_m = 0,\; q_1 + \cdots + q_m = q}^{N_1, \ldots, N_m} \prod_{i=1}^{m} \binom{N_i}{q_i} p_i^{q_i} (1 - p_i)^{N_i - q_i} \,, \tag{19}$$

where m denotes the number of electron shells and N_i the number of electrons within these shells. Formula (19) is readily extended to charge-state correlated events, i.e., k-fold capture associated with l-fold ionisation. However, the straightforward multinomial formulae have a well-known deficiency: They are inappropriate for situations, in which the probability for, e.g., a one-particle transition (such as single capture) is strong, whereas multiple-particle transitions are very unlikely or completely unphysical, as they might correspond to the formation of unstable negative ions.

To overcome this problem, we have introduced an alternative statistical procedure in Ref. [43], which we call the *products-of-binomials* analysis. In this model, the calculated net capture probability $P_{\mathrm{net}}^{\mathrm{cap}}$ is distributed over the physically allowed capture multiplicities $k = 1, \ldots, N_P$ by carrying out binomial statistics on the basis of a new single-particle probability $p^{\mathrm{cap}} \equiv P_{\mathrm{net}}^{\mathrm{cap}}/N_P$. Capture of more electrons than can be accomodated by the projectile is thus eliminated. The charge-state correlated probabilities P_{kl} for k-fold capture with simultaneous l-fold ionisation are then obtained by multiplying the k-fold capture probability

$$P_k^{\mathrm{cap}} = \binom{N_P}{k} (p^{\mathrm{cap}})^k (1 - p^{\mathrm{cap}})^{N_P - k} \tag{20}$$

---

[1]A (modest) step beyond the co-correlation limit was taken recently in Ref. [38].

by independent l-fold binomial ionisation probabilities [calculated according to Eq. (19)]

$$P_{kl} = P_k^{\text{cap}} P_l^{\text{ion}} \ . \tag{21}$$

The products-of-binomials analysis can be viewed as a step beyond the strict IPM, in which the transitions of one electron are not influenced by the transitions of the others, and it has been applied with some success (cf. Secs. 4.1 and 4.3). However, it can also be criticised as it is not based on first-principles arguments and leads to a slight imperfection in the overall probability conservation [43]. We emphasise that a first-principles analysis of the density (11) or the KS orbitals that would go beyond the IPM and would thereby solve the problem of multiple transitions to unphysical final states is highly desirable, but currently not available.

3. Systems with one active electron

For a true single-particle system the most general form of the BGM-states (16) includes powers of the projectile and the target potential

$$|\chi_\nu^{\mu\mu'}\rangle = W_p^\mu W_t^{\mu'}|\phi_\nu^0\rangle \ , \quad \nu = [1, N(U,V)] \ , \ \mu, \mu' = [1, M(U,V)] \ , \tag{22}$$

where $W_{p/t}$ are defined as regularised Coulomb interactions

$$W_t = \frac{1}{r}(1 - \mathrm{e}^{-\epsilon r}) \ , \qquad W_p = \frac{1}{r_p}(1 - \mathrm{e}^{-\epsilon r_p}) \ . \tag{23}$$

In Eq. (23) r and $r_p = |\vec{r} - \vec{R}(t)|$ denote the distances of the electron with respect to the nuclear centres which are separated by the internuclear distance $R(t)$. For the results presented here and in the following sections we apply a simplified representation including only states generated with W_t for antiprotons and W_p for positive projectiles, respectively. The basis states $|\chi_\nu^0\rangle$ [cf. Eq. (16)] are bound (hydrogenic) eigenfunctions, i.e., we identify the set $\{|\chi_v^0\rangle, \nu = 1, \ldots, N\}$ with the set $\{|\phi_v^0\rangle, v = 1, \ldots, V\}$.

Figure 1 shows two extreme situations for the collision system p-H($1s$) calculated with an *identical* basis set. The curves in the correlation diagram are exact solutions of the $(\mathrm{H,H})^+$ quasi-molecule for σ (full line), π (dashed line), and δ (dotted line) orbitals, respectively. The bullets show BGM results for the 16 lowest eigenvalues calculated by diagonalising the molecular Hamiltonian in the BGM basis specified in the figure caption.

The right panel of Fig. 1 illustrates the high-energy behaviour of the total ionisation cross section. The cross section is scaled in such a way that the exact asymptotic result of Bethe-Born perturbation theory corresponds to a horizontal line. Our BGM results merge with this line above 200 keV impact energy. Thus, Fig. 1 shows that the BGM basis is able to bridge the energy range from adiabatic impact energies to the perturbative regime.
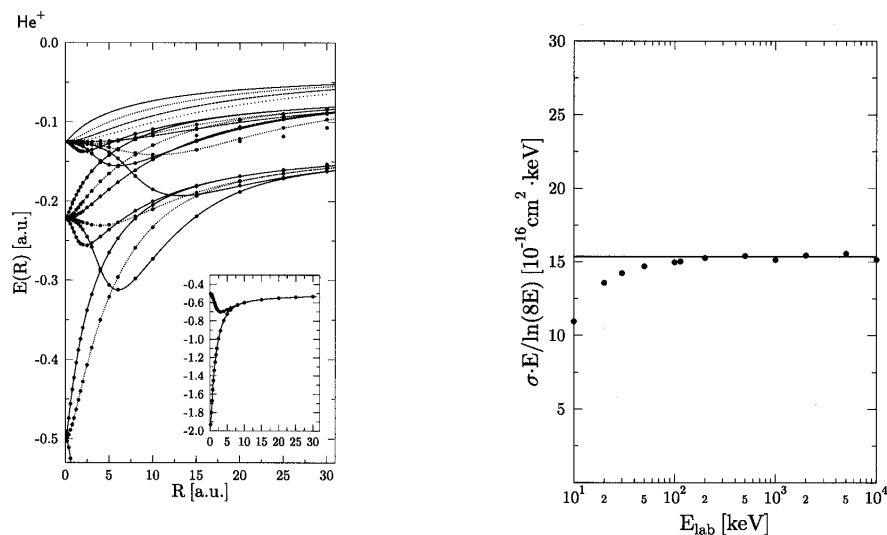
Figure 1. Correlation diagram of $(H,H)^+$ (left panel) and high-energy limit of total ionisation in p-H (right panel) calculated with identical basis sets (22): generating space of hydrogen states $(1s-4f)$ with an 8-fold hierarchy of pseudo-states generated with W_p.

3.1 Ionisation of atomic hydrogen by antiprotons

The collision system $\bar{p}$-H proved to be a benchmark system for an adequate description of ionisation with modern numerical algorithms. The absence of capture permits a single-centred description of the time-dependent wave function which facilitates the investigation of convergence properties significantly.

Figure 2 shows the total cross section for ionisation obtained from a target-centred BGM-basis[2] in comparison with other calculations and the only experimental data set available [45]. Apart from the *continuum distorted wave with eikonal initial-state* (CDW- EIS) calculation [46] which as a perturbative model is not expected to be valid below 100 keV, the more sophisticated basis and grid methods agree within 10% and document the high standard of modern numerical approaches. New experiments will be carried out within the ASACUSA collaboration at CERN and are expected to confirm the relatively large ionisation cross section at small impact energies predicted by theory.

3.2 Capture in collisions between α-particles and Li-like ions

For projectiles with positive charges electron capture is a prominent channel. In the particular case discussed here the $2s$ electron of a lithium-like target ion is captured while the strongly bound K-shell electrons screen the nuclear charge, but remain passive otherwise.

In Fig. 3 we present cross sections for capture in collisions between α-particles and Li-like ions taken from [47]. The Li-like ions are represented at the level

---

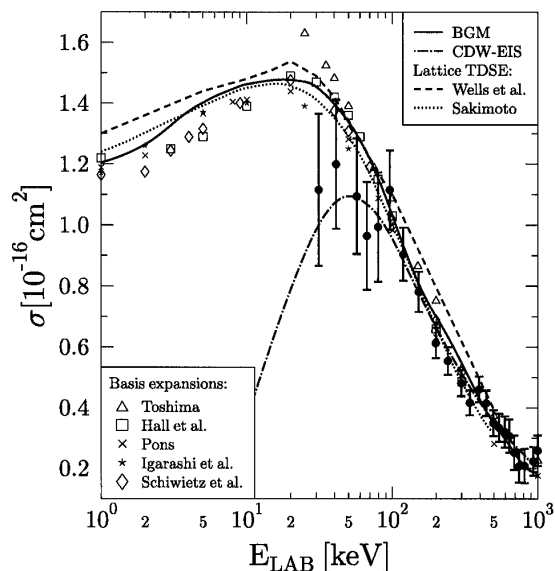[2]these results are better converged than our previous data published in [44].

Figure 2. Total cross section for ionisation of hydrogen by $\bar{p}$ impact as function of impact energy. Theory: present BGM results with hydrogenic states $1s - 4f$ (generating basis), and hierarchy $M = 8$ generated with W_t; CDW-EIS [46], Wells et al. [70], Sakimoto [28], Toshima [68], Hall et al. [69], Pons [27], Igarashi et al. [29], Schiwietz et al. [71] (taken from [69]), Experiment: [45].
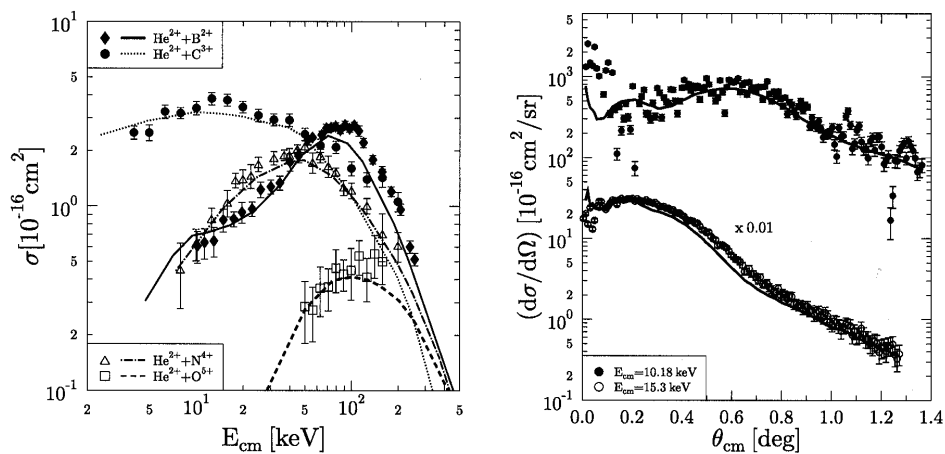

Figure 3. Capture in collisions between α-particles and Li-like ions. Left: Total cross sections for the quasimolecular isoelectronic sequence $(BHe)^{4+}$ to $(OHe)^{7+}$ as functions of impact energy. Right: Differential cross sections for $(BHe)^{4+}$ at the centre of mass energies 10.18 keV and 15.3 keV (multiplied by a factor of 0.01) as functions of the projectile scattering angle. Theory: BGM basis (22) with $N = 20$ and $M = 8$ generated with W_p [47].

of the x-only OPM, with only the 2*s* electron propagated in the Coulomb potential of the α particle and the frozen target potential. The different behaviour within the sequence of total cross sections (left panel) can be attributed to the relation between the quasimolecular energies of the entrance and the dominant capture channels [47]. The differential cross sections (right panel) are calculated using the standard Bessel transform method introduced by McCarrol and Salin [15]. They provide a more sensitive test of theory than total cross sections, as they are known to be very sensitive to spurious effects in conjunction with truncated basis representations. The good agreement between the BGM calculations and the experimental data demonstrates that a fairly accurate separation between the two rearrangement channels, namely capture and ionisation has been achieved.

In summary, the results of this section demonstrate the flexibility of the BGM approach to adapt to different geometric and dynamic situations which are typical for ion-atom collisions.

4. Many-electron systems

The discussion of many-electron systems within the TDKS framework requires first a specification of the KS potential used given that the exact form of the potential is not known. While the x-only OPM can be formulated not only for the static but also for the time-dependent case [48] its implementation is extremely challenging when it comes to the discussion of many-electron problems that involve more than two electrons.

Our works on true many-electron systems are based on a decomposition of the effective electronic interaction contribution v_{ee} of the KS potential into stationary and time-dependent parts [cf. Eq. (13)]

$$
\begin{aligned}
v_{ee}[n](\vec{r}, t) &\equiv v_{\mathrm{H}}[n](\vec{r}, t) + v_{\mathrm{xc}}[n](\vec{r}, t) & (24) \\
&= v_{ee}^0[n_0](r) + \delta v_{ee}[n](\vec{r}, t). & (25)
\end{aligned}
$$

Both parts are then described on different levels of approximation. Such a treatment is not only advantageous from a practical point of view, but also useful for the identification and separation of different physical effects, such as static exchange or dynamical screening effects [10].

For the results presented in this and the following sections we use the x-only OPM for the static potential v_{ee}^0 which depends only on the atomic ground-state density n_0. We consider different approximations for the time-dependent ('response') part δv_{ee}:

- In the simplest scheme, the so-called *no-response* approximation we neglect it completely, i.e., we assume that $\delta v_{ee} = 0$.
- In Ref. [49] we have introduced a global model for time-dependent screening effects, which is built on the assumption that the total KS potential can be represented as the sum of the external projectile potential and a linear combination of ionic target potentials weighted by time-dependent probabilities for the creation of these ions. When the ionic potentials are approximated by the atomic ground state potential which is scaled such that the asymptotic charges of the ions are obtained one arrives at the expression

$$\delta v_{ee}(\vec{r}, t) \approx \delta v_{ee}(r, t) = \frac{-1}{N-1} \sum_{q=1}^{N} (q-1) P_q^{\text{loss}}(t) v_{ee}^0(r). \tag{26}$$

This *target-response* model accounts for the fact that the screening of the target nucleus decreases during the collision when electrons are (partially) removed. One can construct a similar scheme to account also for the time-dependent screening of the projectile ion due to electron capture, but these projectile-response effects turned out to be relatively small (for low and moderately charged ion impact) [50] and will not be considered here.

- For antiproton collisions with He atoms we have recently implemented the full time-dependent OPM potential (which is identical with the time-dependent Hartree-Fock (TDHF) potential in the particular case of a spin-singlet system) [51].

4.1 Single capture in proton collisions with many-electron atoms

Single capture in proton collisions with many-electron atoms seems to be a simple process: one electron is transferred (thereby forming a neutral hydrogen atom) while all other electrons remain passive. However, single capture is difficult to describe in the framework of the IPM, because it contradicts the basic assumption of statistically independent electrons. In reality, only one out of several initially equivalent target electrons can be captured (if the unlikely formation of negative ions is excluded), while in a straight-forward multinomial analysis a non-zero probability for single capture implies non-zero probabilities for higher-order capture events.

As outlined in Sec. 2.3 this problem can be avoided by re-distributing the transferred net probability over $N_P = Z_P$ electrons ($Z_P = 1$ in our case). The results of this products-of-binomials analysis are compared with standard trinomial results and with experiments for single capture associated with zero-fold ionisation (σ_{10}) in *p*-O and *p*-Ne collisions in Fig. 4. In both cases we have included the trinomial double capture results, which overestimate the H$^-$ production cross section at least by an order of magnitude (cf. Fig. 3 of [52]). At the same time the trinomial single-capture cross section is on the low side of the experimental data points in the low-energy regime[3]. Better agreement is obtained in this region with the products-of-binomials analysis, in which the probabilities that correspond to the artifical multiple capture channels are transferred to the single-capture channel.

In the case of oxygen target atoms we observe a significant discrepancy with experiment at energies $E_P > 10$ keV, which has not been understood to the present date. One possible problem of the calculation could be that the x-only OPM potential of atomic oxygen predicts the eigenvalue $\epsilon_{O(2p)}^{\text{OPM}} = -0.614$ a.u. for the $2p$ level, while the first ionisation potential of atomic oxygen amounts to 0.500 a.u. [53]. As the latter equals the binding energy of the H($1s$) state one might expect that a detuning of the condition for resonant capture can affect the results significantly. We have checked this by repeating the capture calculation on the basis of a model potential that is designed to yield a substantially better eigenvalue for O($2p$) [43]. However, these calculations were not successful: the capture cross section turned out too large in the low-energy regime,

---

[3]The *p*-O experiments denoted by the open triangles are believed to be incorrect [43].
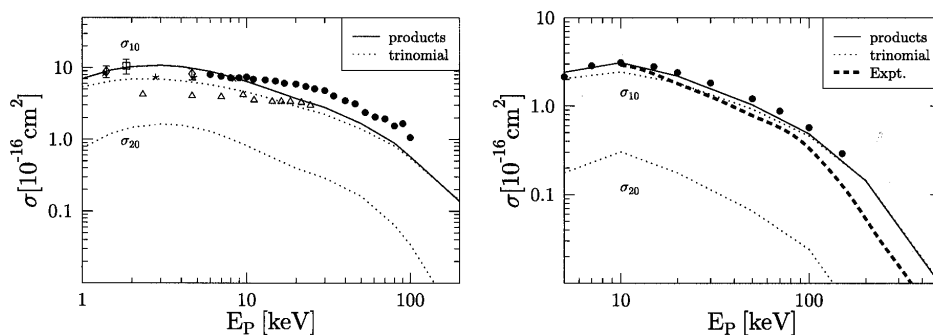
Figure 4. Single (σ_{10}) and double (σ_{20}) capture cross sections as functions of impact energy for *p*-O (left panel) and *p*-Ne (right panel) collisions. Theory: TDKS calculations without target response: *p*-O [43]; *p*-Ne [55]; Experiments: *p*-O [72, 73, 74, 75, 76], cf. [43]; *p*-Ne short-dashed line [52], closed circles, net capture [54].

but did not change significantly above $E_P = 10$ keV.

Another concern might be the open-shell nature of atomic oxygen. We have dealt with the oxygen structure problem on the level of an ensemble-averaging procedure over the partially filled L_{II} shell, which might be too crude an approximation for the description of capture from the spin-triplet ground state configuration ($1s^2\ 2s^2\ 2p^4\ ^3P$). Test calculations show, however, that it is not possible to boost the capture cross section above $E_P = 10$ keV by distributing the four valence electrons other than statistically over the L_{II} shell. This, of course, does not exclude the possibility that the open-shell structure might be responsible for the observed discrepancies. It does indicate, however, that such effects — if present — cannot be taken into account in a simple way.

Finally, we note that response effects, which were not included in the calculations are unlikely to resolve the discrepancies. They have the tendency to *reduce* cross sections for inelastic transitions (see discussion below and in the following sections), and are deemed to be unimportant for the *p*-O collision system.

For Ne target atoms (right panel of Fig. 4) we did check that target response effects [Eq. (26)] are indeed of minor significance. In this case, our results lie above the experimental data for σ_{10} taken from [52]. These data, however, appear to be in conflict with the experimental *net* capture cross section of [54] which is also included in the figure. Net capture consists of pure single capture σ_{10} and the transfer ionisation channels $\{\sigma_{1l},\ l \geq 1\}$ which are, however, too weak to account for the discrepancies between both sets of results [55]. Our calculations clearly favour the data of [54].

Recently, we have extended these capture calculations to *p*-Ar collisions, and have extracted shell- and state-selective cross sections [56]. Figure 5 displays data for capture to the *L* and *M* shells of hydrogen. In both cases we obtain reasonable agreement with the experimental data if we take target-response effects [Eq. (26)] into account. The no-response cross sections are larger except at high energies where the collision is too fast to be sensitive to time-dependent changes of the electronic interaction. It would be of interest to find out whether an improved response model would change the results for H($n = 2$) formation below 10 keV where the shape of the experimental cross section is not reproduced by the present model. For the case of H($n = 3$) formation it should be
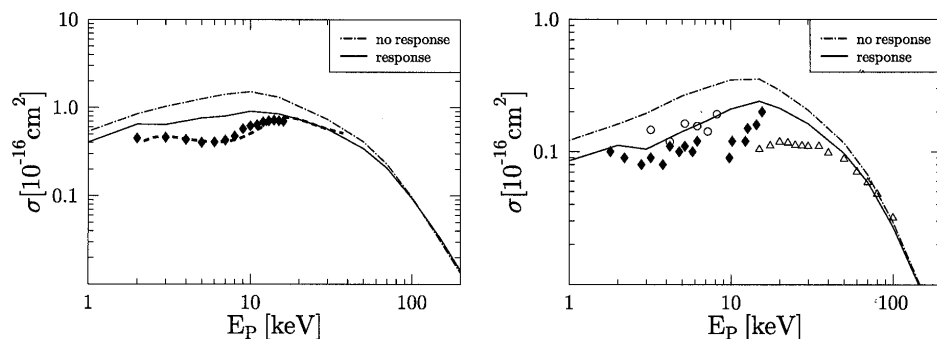
Figure 5. Total cross sections for single capture to the hydrogen *L* (left panel) and *M* shells (right panel) as functions of impact energy for *p*-Ar collisions. Theory: TDKS calculations without and with target response [56]; Experiments: dashed line obtained by fitting to the experimental data summarized in [61], symbols [77, 78, 79, 80, 81], cf. [56].

noted that the experimental data have rather large error bars (see discussion in [56]) and that more accurate experimental data would be necessary to assess the quality of our calculation in closer detail. In any case, the general agreement between the experimental and theoretical data displayed in Fig. 5 is quite remarkable given that the magnitudes of the *L*- and *M*-shell cross sections correspond to a few percent of the total capture only (cf. Fig. 9).

4.2 Ionisation of helium by antiprotons

Another prominent one-electron process in a many-electron collision problem is single ionisation. Single ionisation − in analogy to capture − is inevitably accompanied by multiple ionisation in the IPM. In contrast to the capture case this is not a problem in principle, since multiple ionisation might be weak, but is never forbidden (if we exclude very slow collisions or very tightly bound electrons, for which the impact energy might be too low to remove several electrons). The situation is most transparent when capture processes are completely absent, i.e., if negatively charged projectiles are used. It is thus no surprise that antiproton collisions with noble gas atoms became popular for the investigation of single and multiple ionisation processes and the role of the electron-electron interaction [57].

In particular, $\bar{p}$-He collisions have been studied intensively with explicit two-electron methods and with effective single-particle models. We have addressed this system recently on the level of the x-only OPM, i.e., we have solved the single TDKS equation for the initial He(1*s*) orbital with full account of static and time-dependent screening and exchange effects[4], and have computed single and double-ionisation probabilities and cross sections via the simple limit of Eq. (19) for one shell and two electrons [51].

---

[4]for a spin-singlet system exchange merely compensates the self-interaction contribution in the Hartree potential and is thus identical in TDHF theory and the x-only OPM.

Our results are compared with experiment and with other theoretical data in Fig. 6. For single ionisation we have included only results of two-electron calculations which account for electron correlation effects at least to some extent (for details see [51]). Interestingly, our data are in good agreement with these calculations and appear to bridge the results of the single-centred atomic orbital expansion and forced-impulse methods (denoted as AO1, AO2, and multi-cut FIM) at medium energies with the multi-electron hidden crossing (MEHC) calculation which is expected to yield the correct adiabatic limit. As our model represents the no-correlation limit of the cross section correlation effects cannot be important for single ionisation. Instead, response effects are crucial for energies below 100 keV. Figure 6 includes the comparison with the no-response approximation to illustrate this fact. Comparisons with other single-particle calculations show that the form of the response potential is important and that only the accurate time-dependent x-only model agrees with the two-electron theories [51].

Obviously, there is still a problem concerning the comparison with experiment below 30 keV. As in the case of the $\bar{p}$-H system (cf. Sec. 31) the ASACUSA collaboration will repeat and extend the single (and double) ionisation measurements in the low-energy regime. Based on the results displayed in Fig. 6 the new experiments are expected to correct the older ones and to fall of less steeply towards low energies.

In the case of double ionisation (right panel of Fig. 6) we observe again significant response effects, but obviously our no-correlation limit calculations are not sufficient to explain the data. The only calculation so far that describes these measurements is the multi-cut FIM of [12], which includes static and dynamic correlation effects.

From the TDDFT viewpoint one might ask whether the x-only KS potential or the analysis on the level of the IPM is responsible for the overestimation of the experimental data. Of course, we cannot give a firm answer as long as we cannot include one of these aspects in our calculations. Nevertheless, we believe that the analysis problem is the
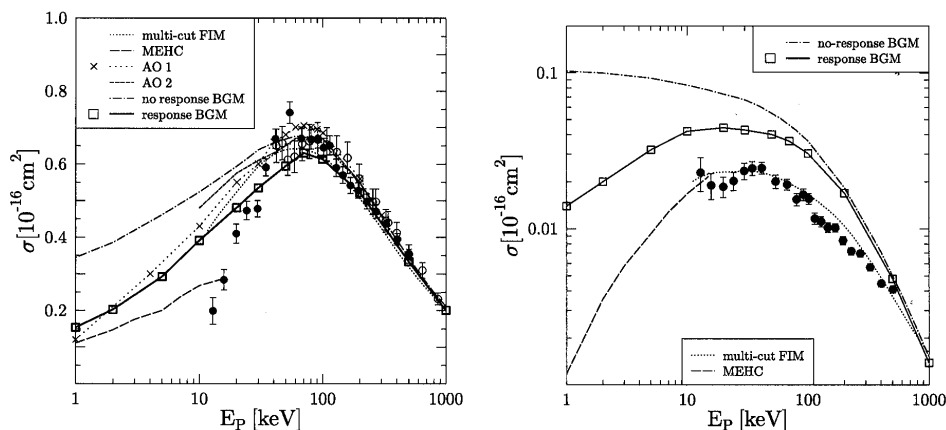

Figure 6. Single (left panel) and double (right panel) ionisation cross sections as functions of impact energy for $\bar{p}$-He collisions. Theory: TDKS calculations without and with response [51]; multi-cut FIM [12], MEHC [82], AO1 [83], AO2 [29]; Experiments: open circles [84], closed circles [85].

major one. As explained in [19, 51] the binomial analysis of single and double ionisation predicts a fixed relation between both observables which is violated in reality. At high impact energies above $E_P \approx 1$ MeV this deficiency becomes apparent when one compares antiproton with proton impact results. One finds that the single-ionisation yields coincide (as is expected from perturbation theory), while the double-ionisation yields are different. This suggests the following conclusion: Though multiple ionisation might be more accessible from the IPM perspective than multiple capture in charge-asymmetric situations, ultimately, a better approximation for the density dependence of *all* multiple-electron observables is strongly desirable.

4.3 Multi-charged recoil ion production and charge-state correlated cross sections

Most of the results presented so far involved one-electron, or effective one-electron problems. The double-ionisation process in a true two-electron system is complicated, and the no-correlation limit of TDDFT (i.e., the IPM) appears to be of limited use in this case. Nevertheless, the situation becomes simpler when more electrons can play an active role, particularly at intermediate and higher energies when the multi-electron events can be considered to be statistical in nature. This is in contrast to what is expected at very low energies, and also in most laser-atom interactions, when multiple ionisation is the result of sequential electron removal. The validity of the IPM approach could be inferred already from semiclassical calculations based on classical trajectories: many results of the N-particle trajectory calculations were reproduced with a model based on the Vlasov equation [58], and numerous experimental findings for multi-electron processes in heavy-ion collisions were explained successfully [34, 41]. However, these semiclassical calculations are not adequate at low and intermediate collision energies, where a quantum approach is required.

TDDFT with a direct interpretation of the KS orbitals is well-suited for the description of direct multiple electron ionisation and capture events. Electronic correlations play a less significant role as compared to the double-ionisation problem in a two-electron system, as there are many pathways leading to a given final charge-state configuration on projectile and target for a given impact parameter and collision energy. The difficulties encountered in the no-correlation limit of TDDFT which were explained in the previous section will arise in the N-electron context for the most violent collision events, i.e., for those channels where (almost) all N electrons are strongly affected.

Much of our work in this area concentrated on neon targets [49, 50], where $N = 10$, and the L-shell is active, furthermore, with oxygen targets we looked at an open-shell system [43], and more recently we have concentrated on argon as a true multi-electron system [56, 59]. First of all, one expects from DFT accurate net cross sections, which can be calculated directly from the density. Recoil ion production is calculated using binomial statistics based on the KS orbitals, and inclusive n-fold capture cross sections can be obtained in an analogous fashion.

As an example of a cross section that depends on the time-evolved density alone we show in Fig. 7 the net electron loss cross section for $\bar{p}$-Ar, p-Ar, and He^{2+}-Ar collisions [59]. The data cover a large range of collision energies: from projectile velocities smaller than the characteristic velocities of outer-shell electrons all the way to the perturbative
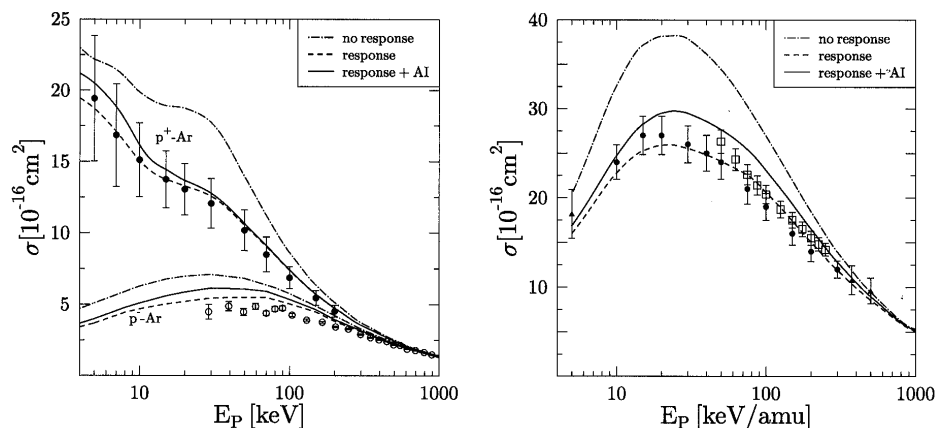
Figure 7. Net electron loss cross sections as functions of impact energy for $\bar{p}$-Ar, p-Ar (both left panel), and He^{2+}-Ar (right panel) collisions. Theory: TDKS calculations without and with target response [59]; also shown are results including response with an estimate of the increase due to autoionising transitions within Ar(M, N). Experiments: $\bar{p}$-Ar [86]; p-Ar [54]; He^{2+}-Ar closed circles [87], closed triangles [88], open squares [89].

regime. From a theoretical perspective the comparison emphasises two points: frst, it shows the effect of dynamical response: calculations with frozen target potentials (no-response model) systematically overestimate electron removal for impact velocities that are roughly below twice the outer electron speeds; secondly, an estimate was made of the contribution of autoionising (AI) transitions, based on the single-particle excitation cross sections included in the TDKS solutions. These estimates are most likely on the high side, as multiple excitations are expected to be weaker than what is predicted from a binomial analysis.

For the case of antiproton projectiles one has the smallest electron removal cross section due to the absence of the charge-transfer channel. Nevertheless, taking 10^{-16} cm^2 as a standard for atomic physics cross sections we observe that the net ionisation cross section is rather high on account of the fact that the Ar(M) shell (which is primarily involved here) has eight electrons to offer for ionisation. Multiple ionisation is not expected to be strong for a singly charged projectile, but it is certainly not negligible.

On the topic of comparison with experiment it should be noted that antiproton beams at low and intermediate energies are difficult to manage, and therefore the cross section is difficult to measure on an absolute scale. If the experimental data are confirmed, and extended to lower energies (work in progress by the ASACUSA collaboration), then they will represent an interesting challenge for TDDFT. This cross section is a measure for how much of the single-electron density remains in the vicinity of the target nucleus. The data are summed over impact parameters, and in the present calculation the net electron loss probabilities are really calculated via the population of bound KS orbitals at the end of the collision. An improvement over the present calculation would involve a more detailed microscopic response, and one could obtain a lowered cross section. An

improved response model can be built along the lines of the recent $\bar{p}$-He calculation [51].

For the proton impact case electron loss from the target is increased dramatically at low energies when compared to antiproton impact due to the presence of electron transfer channels. Electron screening effects are stronger than for $\bar{p}$ impact on an absolute scale, but comparable on a relative scale (typically a 25% effect for impact velocities that match or are below electron speeds in the Ar(M) shell). The theoretical data follow the observed experimental trend of a rising cross section at the lowest energies shown. Charge-exchange is nearly resonant for transfer from Ar(M) into H(1s), and it is this process at the level of the single-particle KS equations that is responsible for this feature in the cross section. Interestingly, response effects at the target do drive the system away from resonance by increasing the Ar(M) shell binding energy during the collision. Nevertheless, their influence on the cross section is not increasing at lower impact energies.

For the case where the charge of the impinging charge is doubled, one can notice a four-fold increase in the electron removal cross section at the highest energies, which is expected from perturbation theory. As the collision energy is reduced the increase in electron removal efficiency becomes less. At 20–30 keV/amu one observes a maximum, and at the lowest energy shown the cross section is slightly lower than for proton impact. At the level of the TDKS equations one may be surprised over this behaviour: the He^{2+} projectile includes more states in its L-shell than H(1s) to accomodate charge transfer from Ar(M), and it pulls with twice the charge. It is, however, only energetically quasi-resonant, i.e., the asymmetry in the single-particle Hamiltonian is much more pronounced in the He^{2+}-Ar than in the $\bar{p}$-Ar case.

Another inclusive cross section that follows directly from the asymptotic density in configuration space is the net ionisation cross section, i.e., one considers only those parts of the density that are neither close to the target nor to the projectile nuclei. In Fig. 8 we show the results for the positive projectile charges $Z_P = 1, 2$ (for antiprotons the result is the same as shown in the previous figure). While comparing the $Z_P = \pm 1$ data we notice that they merge at high energies, where they also agree with the perturbative CDW-EIS calculation of Ref. [60].

The maximum in the result for $Z_P = 1$ is somewhat sharper than in the antiproton case, which is understandable given that at low energies the capture channel competes against ionisation, thereby reducing the cross section for the latter process. At $E_P = 20 - 40$ keV impact energy the calculations including AI corrections assume their maximum values with a ratio of about 4:3 in favour of the $Z_P = 1$ case. In the experiments there is an indication that the maximum occurs at somewhat higher energies. The cross section ratio at the maximum is in agreement with the calculation, but we note that the predicted ionisation cross section is higher than experiment in both instances.

The situation is similar in the case of He^{2+} impact. We note that the cross section is about 2.5 times higher at maximum than in the proton impact case, and that the maximum shifts to a higher collision energy which is in agreement with experiment. The calculation overestimates the experiment (particularly when the more recent data are assumed to be more accurate). This could mean that an improved screening model with more flexibility than just a modified spherically symmetric target potential is needed.
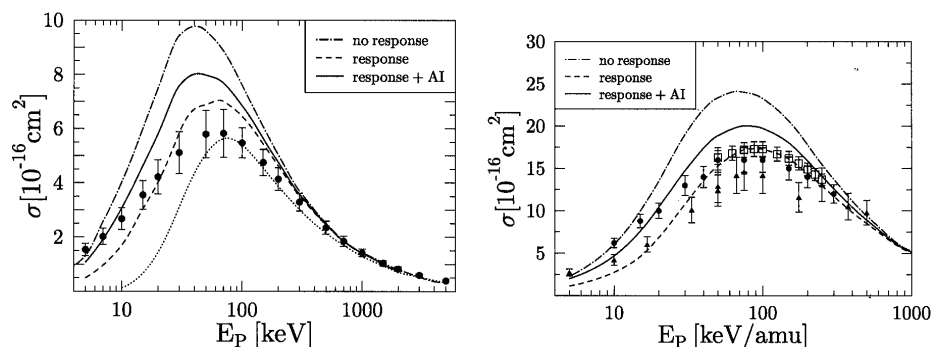
Figure 8. Net ionisation cross sections as functions of impact energy for *p*-Ar (left panel), and He^{2+}-Ar (right panel) collisions. Theory: TDKS calculations without and with target response [59]; also shown are results including response with an estimate of the increase due to autoionising transitions within Ar(*M, N*); dotted line: CDW-EIS calculation [60]. Experiments: *p*-Ar [90]; He^{2+}-Ar closed circles [87], closed triangles [88], open squares [89].

Net capture cross sections are shown for completeness in Fig. 9. The calculations with target response show remarkable agreement with the experiments over a wide range of energies. For the proton impact case we have recently demonstrated that the TDKS calculation is superior to model calculations [61] for both net capture and for capture to the H(*K, L, M*) shells [56]. The different features of the net capture cross sections at low energies together with their explanations have been discussed in the context of the net electron removal cross sections. It is difficult to imagine how a TDDFT calculation not based on the KS scheme, but working directly with the single-particle density and gradients thereof would cope with this problem.

One might conclude then that apart from the minor problems of overestimating the ionisation cross sections all is well with the TDKS calculations based on the exchange-only OPM. Presumably a fine-tuning of the screening effects might resolve the existing
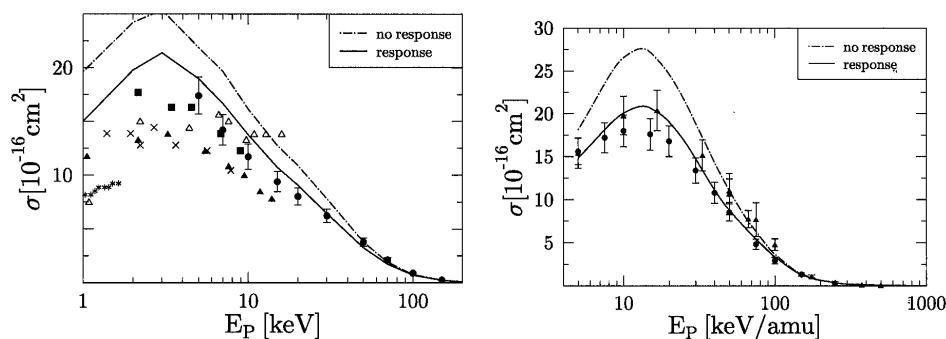

Figure 9. Net capture cross sections as functions of impact energy for *p*-Ar (left panel), and He^{2+}-Ar (right panel) collisions. Theory: TDKS calculations without and with target response [59]; Experiments: *p*-Ar [54, 91, 92, 93, 94, 95], cf. [56]; He^{2+}-Ar closed circles [87], closed triangles [88].

discrepances at low to intermediate energies (where response becomes more important). However, as will be made clear in the next comparisons, some issues remain with the interpretation of the results. The high amounts of charge transfer observed in the calculations at low energies (and shown to agree with experiment) imply that multiple electron transfer does play a substantial role. Therefore, it is worth investigating how the calculations distribute the net probabilities over n-particle channels.

From a theoretical perspective one now faces the following dilemma: In stationary DFT the KS orbitals represent a construct to calculate the single-particle density. In TDDFT one can maintain the same strategy as long as one confines oneself to the computation of net cross sections (which can be computed from the time-evolved density alone). In order to compute q-fold electron loss (or ionisaton, or capture) one can employ binomial statistics which follows from an IPM interpretation of the single-particle density. Within the TDKS scheme it is natural to assume that the orbitals do not just serve as a means to obtain the single-particle density, but that the orbitals in some sense approximate the orbitals of TDHF theory (in reality, in the stationary problem they are closer to the Dyson orbitals [62], and it remains to be investigated what this implies for the time-dependent case).

As outlined in the theory section a straightforward binomial analysis of the impact-parameter-dependent single-particle probabilities leads to predictions of unrealistic multiple electron transfers. In strongly charge-asymmetric systems one faces the problem that a purely statistical evaluation leads to naive predictions for negative ion formation (multiple capture is possible for our $Z_P = 1, 2$ projectiles due to the availability of $N = 18$ electrons in the case of argon targets). An alternative which avoids this problem is the product-of-binomials analysis [43]. This analysis has the tendency to distribute the net probability in such a way that the ($q = 1$)-fold processes are favoured as compared to the higher multiplicities in comparison with binomial analysis. For a detailed comparison of the two methods of evaluating q-fold electron removal in the He^{2+}-Ne system we refer the reader to Ref. [49].

In Fig. 10 we show q-fold electron removal cross sections with $q = 1, \ldots, 4$ and $q = 1, \ldots, 5$ from top to bottom for p-Ar and He^{2+}-Ar, respectively. In the case of proton impact one obtains reasonable agreement at energies above 15 keV for the first three charge states. At the higher collision energies the experimental cross sections for $q = 3, 4$ are dominated apparently by AI events: removal of two electrons from the argon atom at high proton impact energies is likely to involve an L-shell electron which leads to an $L - M$ Auger event. It is remarkable that the $q = 4$ channel predicted on the basis of the IPM to be relatively strong at intermediate energies is completely absent experimentally. At high energies experiment appears to indicate an appreciable $q = 4$ channel fed by Auger cascades. Preliminary results based on a statistical evaluation of these $L - M$ Auger events confirm this interpretation.

For the case of bare helium projectiles we find that the IPM calculation agrees with experiment for $q = 1, \ldots, 4$, while $q = 5$ is completely off. At high energies Ar($q = 3$) production is now dominated by direct ionisation rather than Auger cascades. At energies below 20 keV/amu there is a marked disagreement between calculation and experiment in the $q = 3, 4$ channels which — if true — would mean that a strong violation of IPM behaviour is at work here.
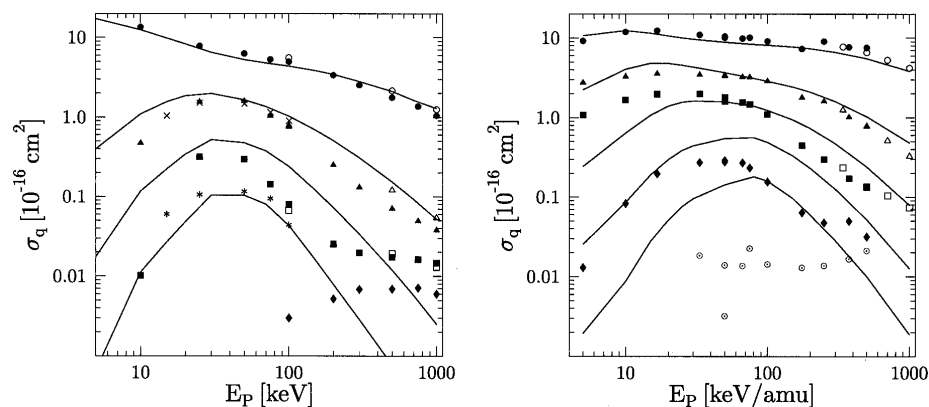
Figure 10. *q*-fold electron loss cross sections as functions of impact energy for *p*-Ar (left panel), and He^{2+}-Ar (right panel) collisions. Theory: TDKS calculations with target response and products-of-binomials analysis [59]; Experiments: *p*-Ar [52, 96, 97], cf. [59]; He^{2+}-Ar [88, 97].

These recoil ion production cross sections demonstrate the following general trend. Depending on the strength of the projectile interaction $q = 1, \ldots, q_0$ electrons can be removed in a direct statistical fashion. The value of q_0 depends on the number of electrons in the outermost shells available for 'easy' removal, and on the projectile charge Z_P. Experimentally we observe $q_0 = 3, 4$ for the two cases $Z_P = 1, 2$, i.e., the cut-off for independent statistically related electron removal events occurs well before the Ar(*M*) shell runs out of electrons. This cannot be described by statistical density-dependent or shell-specific treatments such as the standard binomial and products-of-binomials analyses.

We conclude this section with a discussion of charge-state correlated cross sections. Probabilities for simultaneous capture of k electrons and ionisation of l electrons to produce a ($q = k + l$)-fold charged recoil ion can be calculated either by separating space into three regions and subdividing the single-particle density appropriately (trinomial analysis), or by the products-of-binomials analysis Eq. (21). For the charge-asymmetric situation ($Z_P = 2$ vs $Z_T = 10$) the latter analysis is far superior, especially at lower collision energies.

In Fig. 11 we display cross sections for the He^{2+}-Ne system which correspond to direct multiple ionisation ($k = 0$), single capture with multiple ionisation ($k = 1$) and double capture with multiple ionisation ($k = 2$). The *q*-fold recoil ion production cross sections are reproduced for $q = 1, \ldots, 3$ quite well, and for $q = 4$ the shape is obtained correctly, but the cross section is too high by about a factor of four at all energies [49]. Therefore, only cross sections for up to $q_0 = 4$ are shown.

The comparison of theoretical and experimental cross sections confirms that to a large extent the various channels are indeed correlated statistically. The pure ionisation channels are insignificant at the low energies; the experimental data rise more rapidly than theory. From 50 keV/amu on the agreement is quite good, except that the $l = 4$ channel exhibits a pronounced maximum, while the experimental data appear to be flat.
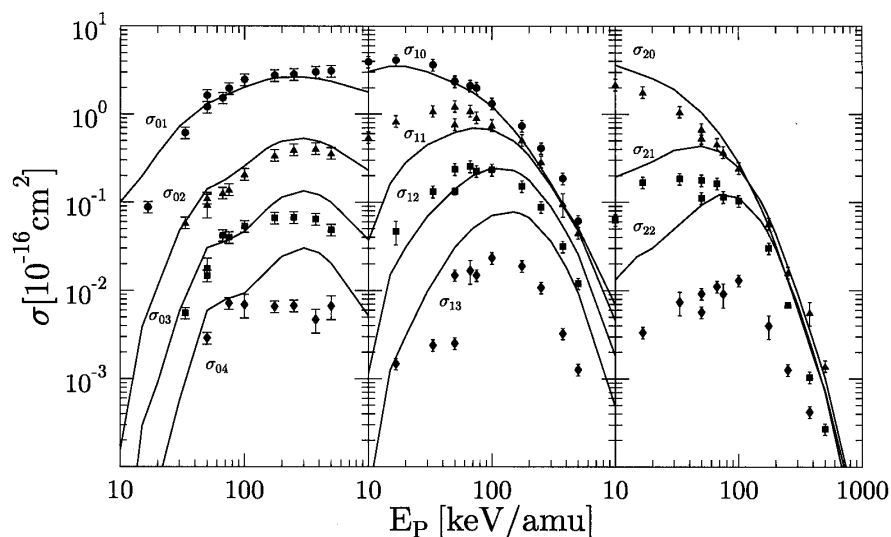
Figure 11. Cross sections for simultaneous k-fold capture and l-fold ionisation as functions of impact energy for He^{2+}-Ne collisions. Left panel: $k = 0$, $l = 1, \ldots, 4$; middle panel: $k = 1$, $l = 0, \ldots, 3$; right panel: $k = 2$, $l = 0, \ldots, 2$. Theory: TDKS calculations with target response and products-of-binomials analysis [49]; Experiments: Ref. [88].

For the case of single capture we notice a good description of pure capture at all energies, but a deficiency of the theory in the ($k = 1$, $l = 1$) channel below 100 keV/amu. It is remarkable that agreement is found for the ($k = 1$, $l = 2$) channel. For triple ionisation accompanying single capture the theory predicts the shape of the cross section, but is too high by a factor of four.

In double capture plus multiple ionisation we overestimate the pure double capture at low energies by about 50%. It is possible that this overestimation is on account of the fact that this process really feeds the ($k = 1$, $l = 1$) channel, i.e., that the separation of projectile bound and continuum states is adequate for single-electron processes, but not when two electrons are involved. The σ_{21} cross section overestimates the data by a factor of two, while σ_{22} is too high by an order of magnitude. Nevertheless, the shape of σ_{22} (E_P) is correct.

This comparison indicates that the prediction of detailed charge-state correlated cross sections is somewhat less reliable than the estimation of the q-fold inclusive processes, in that there can be individual channels which deviate from the statistical distribution employed by the IPM.

Based on these results one might conclude that as long as the single-particle TDKS equations are capable of separating correctly the capture and ionisation probabilities, one can expect the overall picture of the σ_{kl} cross sections to be in agreement with experiment for $q = 1, \ldots, q_0$. We find, however, both confirmation of this conjecture and systematic disagreement in the C^{4+}-Ne system [50] for which $q_0 = 5$. At high energies (above 200 keV/amu) the distribution of q-fold recoil production over multiple

capture and ionisation events is described correctly. However, at lower energies the theory favours single capture accompanied by ionisation over pure ionisation in comparison to experimental data (which are, however, for the F^{4+}-Ne system). Further investigations of the conjecture are definitely needed.

5. Summary

One can summarize this review in the following way. We have demonstrated that the BGM technique for propagating single-electron orbitals represents a reliable method for the calculation of capture and ionisation in intermediate-energy ion-atom and ion-ion collisions with a single active electron.

Then, we have shown applications of the BGM technique to solve the TDKS equations of DFT for low-charge ions colliding with He, O, Ne, and Ar atoms. We have demonstrated the importance of taking into account dynamic response at the target in order to obtain a reasonably accurate time-dependent electron density $n(\vec{r}, t)$.

We have shown that global quantities obtainable directly from the density agree with experimental data. These global quantities are the net ionisation, net capture, and net electron loss cross sections. Furthermore we have illustrated the results for q−fold electron processes. These rely on a statistical interpretation of the calculated density. For the asymmetric collision systems considered in this review, i.e., for systems where the projectile charge is substantially less than the number of electrons on the target the strict no-correlation limit of DFT (multinomial probability distributions) was found to be less reliable than the products-of-binomials analysis. The latter analysis was also applied for the calculation of charge-state-correlated cross sections.

We have found that for a given system involving N target electrons and a projectile charge Z_P total electron multiplicities of $q = 1, \ldots, q_0$ were described well within the IPM framework. The value of q_0 depends on N and to a lesser degree on Z_P. Sometimes, the cross sections for the total electron multiplicity q_0 were reproduced correctly in shape, but were overestimated in magnitude. In the case of $N = 2$ only a sophisticated target response model involving several multipolarities of the density was able to give reasonable results for $q_0 = 2$.

We have mentioned, but not elaborated on applications that require a complete interpretation of the TDKS orbitals in the sense of TDHF theory, i.e., probability analysis of the TDKS calculations at the level of the density matrix. This becomes particularly important for collisions involving electrons on both projectile and target nuclei (cf. Sec. 6.3).

One remaining goal in this programme to investigate the usefulness of the TDDFT approach for ion-atom collisions involves the study of highly charged projectile ions impinging on target atoms involving large numbers of electrons (Ar, Kr, Xe). It will be interesting to see whether the highest multiplicity described successfully by the no-correlation limit of TDDFT, i.e., q_0, will exceed the number of electrons available in the outermost shell. This will represent an even more stringent test of the TDKS equations as a method to provide an accurate electron density than what has been demonstrated so far.

6. Extensions and outlook

Finally, we would like to sketch a few related topics and extensions of our approach that we have considered and which we are planning to elaborate in the future.

6.1 Effective scaling of the net electron loss cross section

Within the target-response approximation [cf. Eq. (26)] we obtained a rather surprising results when we plotted the net electron removal cross section σ_+ for neon target atoms divided by the charge of the projectile Z_P as a function of the projectile energy E_P divided by Z_P for projectile charges ranging from $Z_P = 2, \ldots, 8$ [9, 50]: we found an almost universal curve over a considerable range of reduced energies from some 10 keV$/Z_P$ to a few 100 keV$/Z_P$. This was unexpected particularly for moderate values of E_P / Z_P, since the actual probabilities as a function of impact parameter are rather different, and only the area under the curve bP_+ turned out to be approximately universal. The scaling behaviour was found only in the TDKS calculations with response, but not in the no-response calculations.

Unfortunately, the available experimental data are not sufficiently accurate to prove or disprove the predicted scaling behaviour, so that new experiments with accurate absolute normalisation are needed. From the theoretical viewpoint it might also be interesting to check whether similar scaling behaviours can be found for other targets, e.g., for argon atoms.

6.2 Target excitation processes

The works discussed in the previous sections dealt with ionisation and capture processes. Target excitation was mentioned in Sec. 4.3 only in connection with possible autoionising (AI) multiply-excited states which contribute to electron removal. However, the investigation of excitation processes is also of interest in its own right, both for the general understanding of the (many-) electron dynamics in atomic collisions and for applications, e.g, in atmospheric science [63]. We have carried out detailed calculations for excitation cross sections in p-O collisions [43], which required rather sophisticated analyses based on the LS coupling scheme. We found agreement with available experimental data derived from fluorescence measurements within a factor of two in all cases with one notable exception: for the excitation of the $O(2s\,2p^5\,{}^3P)$ state theory and experiment differed by an order of magnitude. We believe that in this case electron correlation effects are crucial to describe the transition. It is desirable to extend these calculations (and measurements) to other systems in order to clarify the role of electron correlation effects for ion-induced excitation processes. This would also be helpful for more realistic estimates of AI contributions to electron removal.

6.3 Projectiles carrying electrons

Very often in a scattering experiment some electrons are bound to the target and some are bound to the projectile in the entrance channel. If the binding energies of both 'kinds' of electrons are comparable they can get excited, ionised or transferred very much on an equal footing, which implies that one has to take all possible transitions into account at the same time. In recent works we have addressed the He$^+$-Ne collision system as a prototype example. We have shown that one can describe many cross

sections successfully from a simplified viewpoint based on different single-particle calculations for the initial target and projectile electrons [64, 65, 66]. The crucial point is a sensible combination of the indiviual calculations, in particular, an accurate correction for the lack of orthogonality of propagated projectile and target orbitals and an analysis that respects the antisymmetry of the many-electron state. These studies will be pursued further to more complicated situations involving projectiles with more than one active electron.

6.4 Laser-assisted collisions

Very recently an old question gained new momentum: Is it possible to embed an atomic collision experiment in an intense laser field? Such experiments appear to be within reach with present-day technology and are considered in a few laboratories. Several theory groups have started to investigate laser-assisted ion-atom collisions on the basis of advanced numerical techniques. The BGM appears to be a suitable tool for such investigations, and a pilot study on laser-assisted electron transfer indicated that capture probabilities can be considerably enhanced or reduced depending on the temporal synchronisation between projectile and laser fields [67]. These studies will be continued as they may open the door to ultrafast control of electronic motion on the attosecond time scale.

Acknowledgments

References

1. J.S. Yoon and Y.D. Jung, Phys. Plasmas, **6**, 3391 (1999)
2. W.H. Liu and D.R. Schultz, Astrophys. J. **530**, 500 (2000)
3. G. Kraft, Progress in Particle and Nuclear Physics **45**, S473 (2000)
4. J. Ullrich, R. Moshammer, R. Dörner, O. Jagutzki, V. Mergel, H. Schmidt-Böcking, and L. Spielberger, J. Phys. B **30**, 2917 (1997); R. Dörner, V. Mergel, O. Jagutzki, L. Spielberger, J. Ullrich, R. Moshammer, and H. Schmidt-Böcking, Phys. Rep. **330**, 95 (2000)
5. J. Ullrich, R. Moshammer, A. Dorn, R. Dörner, L.Ph.H. Schmidt, and H. Schmidt-Böcking, Rep. Prog. Phys. **66**, 1463 (2003)
6. M. Chassid and M. Horbatsch, J. Phys. B **31**, 515 (1998); Phys. Rev. A **66**, 012714 (2002)
7. D.H. Madison, M. Schulz, S. Jones, M. Foster, R. Moshammer, and J. Ullrich, J. Phys. B **35**, 3297 (2002)
8. R.D. Rivarola and P.D. Fainstein, Nucl. Inst. Meth. B **205**, 448 (2003)

9. H.J. Lüdde, T. Kirchner, and M. Horbatsch: Quantum Mechanical Treatment of Ion Collisions with Many-Electron Atoms. In: *Photonic, Electronic, and Atomic Collisions*, ed. by J. Burgdörfer, J. Cohen, S. Datz, and C.R. Vane (Rinton Press, Princeton 2002)

10. T. Kirchner: Electron−Interaction Effects in Ion-Induced Rearrangement and Ionization Dynamics: A Theoretical Perspective. In: *Many-Particle Quantum Dynamics in Atomic and Molecular Fragmentation*, ed. by J. Ullrich and V.P. Shevelko (Springer, Berlin, Heidelberg, New York 2003)

11. A.L. Godunov and J.H. McGuire, J. Phys. B **34**, L223 (2001)

12. T. Bronk, J.F. Reading, and A.L. Ford, J. Phys. B **31**, 2477 (1998)

13. C. Díaz, F. Martín, and A. Salin, J. Phys. B **33**, 4373 (2000)

14. B.H. Bransden and M.R.C. McDowell: *Charge Exchange and the Theory of Ion-Atom Collisions* (Clarendon Press, Oxford 1992)

15. R.D. McCaroll and A. Salin, J. Phys. B **1**, 163 (1968)

16. E.K.U. Gross, J.F. Dobson, and M. Petersilka: Density Functional Theory of Time-Dependent Phenomena. In: *Topics in Current Chemistry 181*, ed. by R.F. Nalewajski (Springer, Berlin, Heidelberg, New York 1996)

17. K. Burke and E.K.U. Gross: A Guided Tour of Time-Dependent Density Functional Theory. In: *Density Functionals: Theory and Applications, Proceedings of the Tenth Chris Engelbrecht Summer School in Theoretical Physics*, ed. by D. Joubert (Springer, Berlin, Heidelberg, New York 1997)

18. N.T. Maitra, K. Burke, H. Appel, E.K.U. Gross, and R. van Leeuwen: Ten Topical Questions in Time-Dependent Density Functional Theory. In: *Review in Modern Quantum Chemistry: A Celebration of the Contributions of R.G. Parr*, ed. by K.D. Sen (World Scientific, Singapore 2001)

19. H.J. Lüdde: Time-Dependent Density Functional Theory in Atomic Collisions. In: *Many-Particle Quantum Dynamics in Atomic and Molecular Fragmentation*, ed. by J. Ullrich and V.P. Shevelko (Springer, Berlin, Heidelberg, New York 2003)

20. R.M. Dreizler and E.K.U. Gross: *Density Functional Theory* (Springer, Berlin, Heidelberg, New York 1990)

21. E. Runge and E.K.U. Gross, Phys. Rev. Lett. **52**, 997 (1984)

22. J.D. Talman and W.F. Shadwick, Phys. Rev. A **14**, 36 (1976)

23. E. Engel and R.M. Dreizler, J. Comp. Chem. **20**, 31 (1999)

24. D.R. Schultz, M.R. Strayer, and J.C. Wells, Phys. Rev. Lett. **82**, 3976 (1999)

25. D.C. Ionescu and A. Belkacem, Phys. Scr. **T80**, 128 (1999)

26. A. Kolakowska, M. Pindzola, F. Robicheaux, D.R. Schultz, and J.C. Wells, Phys. Rev. A **58**, 2872 (1998); A. Kolakowska, M. Pindzola, and D.R. Schultz, Phys. Rev. A **59**, 3588 (1999)

27. B. Pons, Phys. Rev. A **63**, 012704 (2001); ibid. **64**, 019904 (2001)

28. K. Sakimoto, J. Phys. B **33**, 5165 (2000)

29. A. Igarashi, S. Nakazaki, and A. Ohsaki, Phys. Rev. A **61**, 062712 (2000)

30. X.M. Tong, D. Kato, T. Watanabe, and S. Ohtani, Phys. Rev. A **62**, 052701 (2000)

31. J. Fu, M.J. Fitzpatrick, J.F. Reading, and R. Gayet, J. Phys. B **34**, 15 (2001); E.Y. Sidky, C. Illescas, and C.D. Lin, Phys. Rev. Lett. **85**, 1634 (2000); N. Toshima, Phys. Rev. A **59**, 1981 (1999)

32. E.A. Solov'ev, Sov. Phys. Usp. **32**, 228 (1989); M. Pieksma and S.Y. Ovchinnikov, J. Phys. B **27**, 4573 (1994)

33. C.L. Cocke and R.E. Olson, Phys. Rep. **205**, 163 (1991)

34. M. Horbatsch, Phys. Rev. A **49**, 4556 (1994)

35. C. Illescas and A. Riera, Phys. Rev. A **60**, 4546 (1999)

36. H.J. Lüdde, A. Henne, T. Kirchner, and R.M. Dreizler, J. Phys. B **29**, 4423 (1996)

37. O.J. Kroneisen, H.J. Lüdde, T. Kirchner, and R.M. Dreizler, J. Phys. A **32**, 2141 (1999)

38. M. Petersilka and E.K.U. Gross, Laser Phys. **9**, 105 (1999)

39. H.J. Lüdde and R.M. Dreizler, J. Phys. B **18**, 107 (1985)
40. T. Kirchner, L. Gulyás, H.J. Lüdde, E. Engel, and R.M. Dreizler, Phys. Rev. A **58**, 2063 (1998)
41. M. Horbatsch, Phys. Lett. A **187**, 185 (1994)
42. V. Shevelko and H. Tawara: *Atomic Multielectron Processes* (Springer Berlin 1998)
43. T. Kirchner, H.J. Lüdde, M. Horbatsch, and R.M. Dreizler, Phys. Rev. A **61**, 052710 (2000)
44. T. Kirchner, H.J. Lüdde, O.J. Kroneisen, and R.M. Dreizler, Nucl. Inst. Meth. B **154**, 46 (1999)
45. H. Knudsen, U. Mikkelsen, K. Paludan, K. Kirsebom, S.P. Møller, E. Uggerhøj, J. Slevin, M. Charlton, and E. Morenzoni, Phys. Rev. Lett. **74**, 4627 (1995)
46. D.R. Schultz, P.S. Krstić, C.O. Reinhold, and J.C. Wells, Phys. Rev. Lett **76**, 2882 (1996)
47. D. Skiera, R. Trassl, K. Huber, H. Bräuning, E. Salzborn, M. Keim, A. Achenbach, T. Kirchner, H.J. Lüdde, and R.M. Dreizler, Phys. Scr. **T92**, 423 (2001)
48. C.A. Ullrich, U.J. Gossmann und E.K.U. Gross, Phys. Rev. Lett. **74**, 872 (1995)
49. T. Kirchner, M. Horbatsch, H.J. Lüdde, and R.M. Dreizler, Phys. Rev. A **62**, 042704 (2000)
50. T. Kirchner, M. Horbatsch, and H.J. Lüdde, Phys. Rev. A **64**, 012711 (2001)
51. M. Keim, A. Achenbach, H.J. Lüdde, and T. Kirchner, Phys. Rev. A **67**, 062711 (2003)
52. R.D. DuBois and S.T. Manson, Phys. Rev. A **35**, 2007 (1987)
53. A.A. Radzig and B.M. Smirnov, *Reference Data on Atoms, Molecules, and Ions*, Springer Series in Chemical Physics Vol. 31 (Springer, Berlin, 1985)
54. M.E. Rudd, R.D. DuBois, L.H. Toburen, C.A. Ratcliffe, and T.V. Goffe, Phys. Rev. A **28**, 3244 (1983)
55. T. Kirchner, H.J. Lüdde, and R.M. Dreizler, Phys. Rev. A **61**, 012705 (2000)
56. T. Kirchner, M. Horbatsch, M. Keim, and H.J. Lüdde, Phys. Rev. A **68**, in press (2003)
57. H. Knudsen and J.F. Reading, Phys. Rep. **212**, 1 (1992)
58. M. Horbatsch, J. Phys. B **25**, 3797 (1992)
59. T. Kirchner, M. Horbatsch, and H.J. Lüdde, Phys. Rev. A **66**, 052719 (2002)
60. T. Kirchner, L. Gulyás, H.J. Lüdde, A. Henne, and R.M. Dreizler, Phys. Rev. Lett. **79**, 1658 (1997)
61. A. Amaya-Tapia, H. Martínez, R. Hernández-Lamoneda, and C.D. Lin, Phys. Rev. A **62**, 052718 (2000)
62. O.V. Gritsenko, B. Braida, and E.J. Baerends, J. Chem. Phys. **119**, 1937 (2003)
63. M.H. Rees: *Physics and Chemistry of the Upper Atmosphere* (Cambridge University Press, Cambridge 1989)
64. T. Kirchner and M. Horbatsch, Phys. Rev. A **63**, 062718 (2001)
65. T. Kirchner, H.J. Lüdde, and M. Horbatsch: Nonperturbative Study of the Re-arrangement Dynamics in Ion-Atom Collisions with Active Electrons on Projectile and Target. In: *Proceedings of the 23rd International Conference on Photonic, Electronic, and Atomic Collisions*, ed. by R. Schuch et al., to be published in 2004
66. T. Kirchner, M. Horbatsch, and H.J. Lüdde, submitted to Phys. Rev. Lett. (2003)
67. T. Kirchner, Phys. Rev. Lett. **89**, 093203 (2002)
68. N. Toshima, Phys. Rev. A **64**, 024701 (2001)
69. K.A. Hall, J.F. Reading, and A.L. Ford, J. Phys. B **29**, 6123 (1996)
70. J.C. Wells, D.R. Schultz, P. Gavras and M.S. Pindzola, Phys. Rev. A **54**, 593 (1996)
71. G. Schiwietz, U. Wille, R. Muiño Díez, P.D. Fainstein, and P.L. Grande, J. Phys. B **29**, 307 (1996)
72. W.R. Thompson, M.B. Shah, and H.B. Gilbody, J. Phys. B **29**, 725 (1996)
73. I.D. Williams, J. Geddes, and H.B. Gilbody, J. Phys. B **17**, 1547 (1984)
74. R.F. Stebbings, A.C.H. Smith, and H. Ehrhardt, J. Geophys. Res. **69**, 2349 (1964)
75. B. van Zyl and T.M. Stephen, in *Proceedings of the 17th International Conference on the Physics of Electronic and Atomic Collisions, Brisbane 1991*, edited by I.E. McCarthy, W.R. MacGillivray, and M.C. Standage, (Griffith University, Brisbane, 1991)

76. B.G. Lindsay, D.R. Sieglaff, D.A. Schafer, C.L. Hakes, K.A. Smith, and R.F. Stebbings, Phys. Rev. A **53**, 212 (1996)
77. J.S. Risley, F.J. de Heer, and C. B. Kerkdijk, J. Phys. B **11**, 1759 (1978)
78. R.H. Hughes, H.R. Dawson, B.M. Doughty, D. B. Kay, and C. A. Stigers, Phys. Rev. **146**, 53 (1966)
79. R.H. Hughes, C.A. Stigers, B.M. Doughty, and E. D. Stokes, Phys. Rev. A **1**, 1424 (1970)
80. H.R. Dawson and D.H. Loyd, Phys. Rev. A **9**, 166 (1974)
81. H.R. Dawson and D.H. Loyd, Phys. Rev. A **15**, 43 (1977)
82. G. Bent, P.S. Krstić, and D.R. Schultz, J. Chem. Phys. **108**, 1459 (1998)
83. T.G. Lee, H.C. Tseng, and C.D. Lin, Phys. Rev. A **61**, 062713 (2000)
84. L.H. Andersen, P. Hvelplund, H. Knudsen, S.P. Møller, O.P. Pedersen, S. Tang-Petersen, E. Uggerhøj, K. Elsener, and E. Morenzoni Phys. Rev. A **41**, 6536 (1990)
85. P. Hvelplund, H. Knudsen, U. Mikkelsen, E. Morenzoni, S. P. Møller, E. Uggerhøj, and T. Worm J. Phys. B **27**, 925 (1994)
86. K. Paludan, H. Bluhme, H. Knudsen, U. Mikkelsen, S.P. Møller, E. Uggerhøj, and E. Morenzoni, J. Phys. B **30**, 3951 (1997)
87. M.E. Rudd, T.V. Goffe, and A. Itoh, Phys. Rev. A **32**, 2128 (1985)
88. R.D. DuBois, Phys. Rev. A **36**, 2585 (1987)
89. L.J. Puckett, G.O. Taylor, and D.W. Martin, Phys. Rev. **178**, 271 (1969)
90. M.E. Rudd, Y.K. Kim, D.H. Madison, and J.W. Gallagher, Rev. Mod. Phys. **57**, 965 (1985)
91. S. K. Allison, Rev. Mod Phys. **30**, 1137 (1958)
92. J.F. Williams and D.N.F. Dunbar, Phys. Rev. **149**, 62 (1966)
93. B.J.H. Stedeford and J.B. Hasted, Proc. R. Soc. London, Ser. A, **227**, 466 (1955)
94. Yu.S. Gordeev and M.N. Panov, Zh. Tekh. Fiz. **34**, 857 (1964) [Sov. Phys. Tech. Phys. **9**, 656 (1964)]
95. Z.Z. Latypov and A.A. Shaporenko, Zh. Tekh. Fiz. **46**, 2178 (1976) [Sov. Phys. Tech. Phys. **21**, 1277 (1976)]
96. R.D. DuBois, L.H. Toburen, and M.E. Rudd, Phys. Rev. A **29**, 70 (1984)
97. L.H. Andersen, P. Hvelplund, H. Knudsen, S.P. Møller, A.H. Sørensen, K. Elsener, K.-G. Rensfelt, and E. Uggerhøj, Phys. Rev. A **36**, 3612 (1987)